超低功率之高頻砷化銦通道高電子遷移率電晶體之研究

研究生：張家源　　　　　指導教授：張 翼 博士

國立交通大學材料科學與工程研究所

中文摘要

在本論文中，高效率的砷化銦通道高電子遷移率電晶體被製造並評估其高頻、低功率消耗的應用。使用次微米線寬閘極與最佳化的磊晶結構，大幅提昇了砷化銦通道高電子遷移率電晶體元件特性。在本論文中也詳細探討元件佈局對整體特性的影響。

本論文中砷化銦鋁/砷化銦鎵功率高電子遷移率電晶體在使用 70 奈米的 T 型閘極與 double δ-doping 之元件也被成功的製作與研究。因具備奈米尺寸的閘極與銦含量高達 60%的通道層，此電晶體具有 890 mA/mm 的飽和汲極-源極電流以及 827mS/mm 的轉導值，並展現 200GHz 的高截止頻率(f_T)與 300GHz 的最高震盪頻率(f_{max})。此元件在 32 GHz 之 Ka 頻段下具有良好的特性，表現出 14.5 dBm (176 mW/mm) 的最大輸出功率對應 11.1dBm (80 mW/mm) 的 P1dB，以及 9.5dB 的功率增益。

為了進一步提昇元件特性，通道層的銦含量提高到百分之百成了砷化銦通道

1896

高電子遷移率電晶體，當元件操作在0.7伏特的低偏壓時，砷化銦的高速特性使得元件的截止頻率被提升到310 GHz而最高震盪頻率也提高到了330 GHz，而內部的延遲時間只有0.63兆分之一秒。另一方面在量測時過高的操作偏壓會伴隨著載通道層內的載子撞擊離子化現象，此一現象會造成元件特性劣化。因此元件操作時必須避免撞擊離子化現象以得到最好的操作特性。此元件經過評估後，展現出高速、低消耗功率邏輯應用的潛力。

為了符合超低消耗功率的需求，我們評估了砷化銦通道高電子遷移率電晶體在超低功率低雜音放大器的應用。在0.2伏特的低電壓操作下，透過小訊號S參數量測此元件展現出120 GHz的高截止頻率以及157 GHz的最高震盪頻率。在消耗功率只有1.2 mW的偏壓條件與12 GHz的操作頻率下，元件展現出9.7dB的高增益以及0.8dB的低雜音指數。與其他的砷化銦鎵通道層元件相比，本論文中的砷化銦元件展現出較高的增益以及較低的雜音指數。此結果指出砷化銦元件適用於超低功率的太空雷達、攜帶用毫米波通訊裝置與手持影像裝置等應用。

為了延續摩爾定律、找尋下一世代取代矽互補式金氧半導體電晶體的替代品，應用原子層沈積法所成長的氧化鋁被使用在砷化銦高電子遷移率電晶體上當作閘極介電層。比較氧化鋁極介電層使用前與使用後，可找出元件的最佳磊晶結構以符合高速、低消耗功率的需求。

The Study of InAs-Channel High Electron Mobility Transistors for High Frequency and Ultra-Low Power Applications

Student: Chia-Yuan Chang Advisor: Dr. Edward Yi Chang

Department of Materials Science and Engineering

National Chiao Tung University

Abstract

High performance InAs-channel high electron mobility transistors (HEMTs) have been fabricated and characterized for high frequency and high speed logic low-power consumption applications. The performance of the InAs-channel HEMTs was improved by optimizing the device structure and using a sub-micron gate. The epi-structure, layout design and electrical measurements of the devices are discussed in details in this dissertation.

In this study, a 70-nm $In_{0.52}Al_{0.48}As/In_{0.6}Ga_{0.4}As$ power MHEMT with double δ-doping was fabricated and evaluated. The device has a high transconductance of 827 mS/mm. The saturated drain-source current of the device is 890 mA/mm. A current gain cutoff frequency (f_T) of 200 GHz and a maximum oscillation frequency (f_{max}) of 300 GHz were achieved due to the nanometer gate length used and the high Indium content in the channel. When measured at 32 GHz, the $0.07 \times 160\ \mu m^2$ device

demonstrates maximum output power of 14.5 dBm (176 mW/mm) and P1dB of 11.1 dBm (80 mW/mm) with 9.5 dB power gain. The excellent DC and RF performance of the 70-nm MHEMT shows a great potential for Ka-band power applications.

In order to further enhance the performance, the indium content of the $In_xGa_{1-x}As$ channel was increased to 100 % to form an InAs-channel HEMT. A high current gain cutoff frequency (f_t) of 310 GHz and a high maximum oscillation frequency (f_{max}) of 330 GHz were obtained at V_{DS} = 0.7 V due to the high electron mobility in the InAs channel. Performance degradation was observed on the cutoff frequency (f_t) and the corresponding gate delay time for logic applications caused by impact ionization due to a low energy bandgap in the InAs channel. DC and RF characterizations on the device have been performed to determine the proper bias conditions in avoidance of the performance degradations due to the impact ionization. With the design of InGaAs/InAs/InGaAs composite channel, the impact ionization was not observed until the drain bias reached 0.7 volt, and at this bias the device demonstrated very low gate delay time of 0.63 psec. The high performance of the InAs/InGaAs HEMTs demonstrated in this study shows its great potential for high speed and very low power logic applications.

In the issue of power consumption, InAs-channel HEMT for ultralow-power low-noise amplifier (LNA) applications has been characterized. Small-signal

S-parameter measurements performed on the InAs-channel HEMT at a low drain-source voltage of 0.2 V exhibited an excellent f_T of 120 GHz and an f_{max} of 157 GHz. At an extremely low level of dc power consumption of 1.2 mW, the device demonstrated an associated gain of 9.7 dB with a noise figure of less than 0.8 dB at 12 GHz. Such a device also demonstrated a higher associated gain and a lower noise figure than other InGaAs-channel HEMTs at extremely low dc power consumption. These results indicate the outstanding potential of InAs-channel HEMT technology for ultralow-power space-based radar, mobile millimeter-wave communications and handheld imager applications.

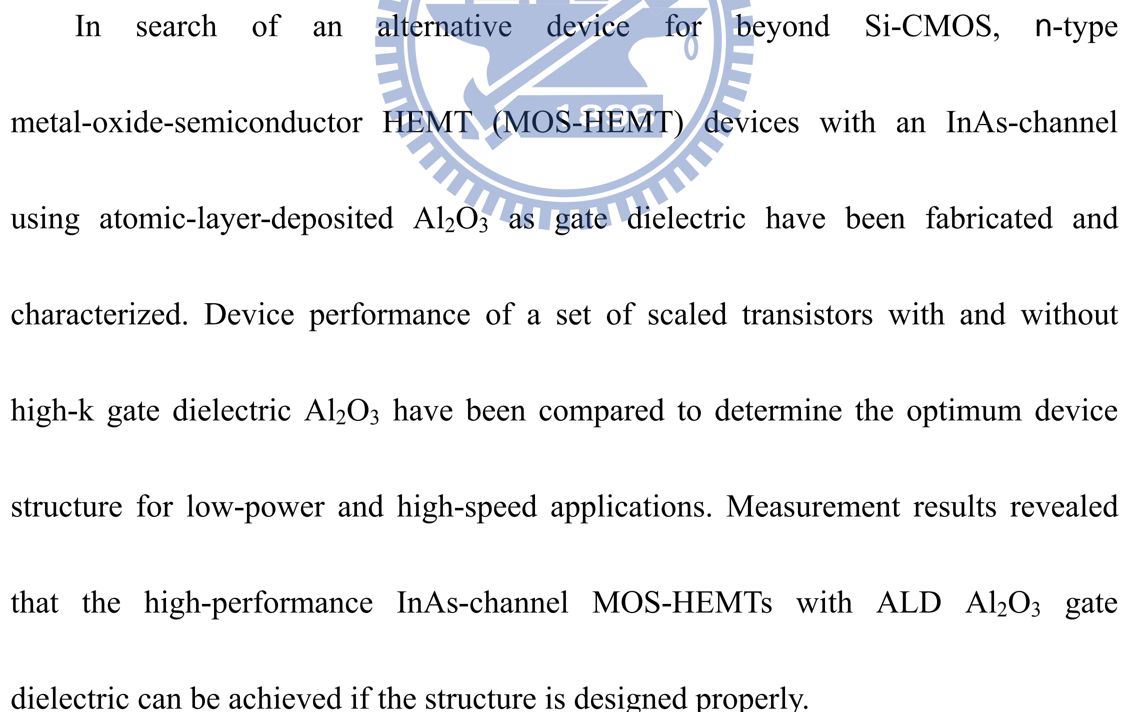

In search of an alternative device for beyond Si-CMOS, n-type metal-oxide-semiconductor HEMT (MOS-HEMT) devices with an InAs-channel using atomic-layer-deposited Al_2O_3 as gate dielectric have been fabricated and characterized. Device performance of a set of scaled transistors with and without high-k gate dielectric Al_2O_3 have been compared to determine the optimum device structure for low-power and high-speed applications. Measurement results revealed that the high-performance InAs-channel MOS-HEMTs with ALD Al_2O_3 gate dielectric can be achieved if the structure is designed properly.

誌　謝

在完成本論文之後，首先我要感謝的是我的指導教授張翼博士。在我進入交通大學後引領我進入砷化鎵高頻元件的領域。在張翼老師的實驗室裡不僅使用全台灣最好的實驗儀器與設備，在老師的安排下訪問國外優秀的研究單位學、提昇自我的能力。經過老師多年的悉心指導，即使在日本電信公司 NTT 研究所做研究，讓我的外語溝通能力與研究能力都能不遜色於當地的研究員。在交通大學材料科學與工程研究所的日子，我感受到張翼教授幽默風趣並具有特色的指導方式與實驗室溫馨的研究氣氛，這個難得可貴的經歷與學習經驗，讓我受用無窮。

在這裡我也感謝元智大學的許恆通教授，謝謝他對我研究上的指導與幫助。也要感謝交大實驗室的連亦中學長、陳仕鴻博士、林越欽博士、李澤倫先生、王勝評先生、褚立新學長、謝炎章學長、陳俊淇學長在實驗上的幫助及建議。感謝國家奈米元件實驗室(NDL)及交大奈米中心(前半導體中心)，同時提供優良的儀器設備與環境，使實驗能夠更加順利進行。特別要感謝的是與張翼教授有合作關係之東京工業大學(TITech)的 Yasuyuki Miyamoto 教授以及日本 NTT 物性科學基礎研究所的 Yamaguchi 博士，對我在日本東京與神奈川做研究時的關心照顧以及實驗上的協助。

另外我也要感謝同窗多年的郭建億同學、呂宗育同學，一起陪伴我走過六年多的博士班生活，相信許多年後我們會懷念起一起窩在無塵室裡的時光。感謝詹前璋先生在儀器設備及廠務方面的幫忙。感謝陳克弦學長、林龔樑學長、唐士軒學弟、張羅恆學長、蕭佑霖學弟、黃偉進學弟、蘇詠萱學妹以及其他學弟妹們的幫助。另外要感謝秘書李安蕙小姐與黃琳婷小姐，還有之前的歷任秘書小姐，謝謝你們的幫助。

最後，我要感謝我的爸爸、媽媽，謝謝您的支持與包容，讓我終於可以完成我的博士學位，感謝兩個哥哥有你們的支持我才可以無後顧之憂的專注於課業，

希望你們一起分享我的榮耀。

Contents

Abstract (in Chinese)……………………………………………………….i

Abstract (in English)………………………………………………………iii

Acknowledge (in Chinese)…………………………………………………vi

Contents……………………………………………………………………viii

Table Captions……………………………………………………………..xi

Figure Captions……………………………………………………………xii

Chapter 1 Introduction……………………………………………………1

1.1The Background and Motivation………………………………………….1

1.2 Overview of High Electron Mobility Transistors (HEMTs)……..……………..2

1.3 Sub-micron Gate Definition ……………………………………..………....3

1.4 Outline of the Dissertation……..……………………………………………....5

Chapter 2 Fabrication of $In_xGa_{1-x}As$ High Electron Mobility Transistors ……………………………… …………………………12

2.1 Material Properties and Growth of HEMT…………………………….12

2.2 Device Fabrication……….……………………………………….......……12

2.2.1 Mesa isolation……………………………………………………………13

2.2.2 Ohmic contact Formation………………………………………..………………...14

2.2.3 T-shaped gate and Recess process………………..………………………14

2.2.4 Device passivation and contact via formation……..…………………………15

2.3 Airbridge formation….……………….……….……………………….………..16

Chapter 3 DC and RF Measurements of InGaAs Metamorphic High Electron Mobility Transistor……………………………..……..……....29

3.1 Device Characterization……………………………………………………..29

3.2 DC characteristics………………………………………………….……...30

3.2.1 I-V characteristics………………………….…………………………...30

3.2.2 Transmission line model (TLM)……………….……………………….....33

3.2.3 Breakdown characteristics……………….……………………………...34

3.3 RF Characteristics & Measurements…………………...…………………...…35

3.3.1 Scattering parameters………………………...……………………...35

3.3.2 Current gain cutoff frequency f_T……..……………...……………………...36

3.3.3 Maximum frequency of oscillation f_{max}………..………...…………………...38

3.3.4 Noise figure……..……………………………..………...…………………...40

3.3.5 RF measurement calibration…….…………..………...…………………...42

Chapter 4 High-Performance $In_{0.52}Al_{0.48}As/In_{0.6}Ga_{0.4}As$ Power Metamorphic High Electron Mobility Transistor for Ka-Band Applications……………………………………………….……….....48

4.1 Introduction……………………………………………………………….48

4.2 Experiments…………………………………………………………….....49

4.3 Device Performance………………….....…………………………………49

4.4 Conclusion………………...………………………………………………50

Chapter 5 Investigation of Impact Ionization in InAs-Channel HEMT for High Speed and Low Power Applications……...……....57

5.1 Introduction……………………...………………………………………..57

5.2 Device Fabrication……………………...…………………………...……58

5.3 Results and Discussion……………..……………………………………….59

5.4 Conclusion………………………………...……………………………61

Chapter 6 InAs-Channel High-Electron-Mobility Transistors for Ultralow-Power Low Noise Amplifier Applications……….........69

6.1 Introduction……………………..…………………………..…………69

6.2 Material Growth and Device Fabrication…………….……………...…70

6.3 Experimental Results and Discussion…………………..……..………....71

6.4 Conclusion……………………………..…………………………………..72

Chapter 7 InAs-Channel Metal-Oxide-Semiconductor HEMTs with Atomic Layer Deposited Al_2O_3 Gate Dielectric………..………….82

7.1Introduction……………………..…………………………..…………82

7.2 Experimental…………………………………………………………….83

7.3 Results and Discussion…………..……………………….……….....84

7.4 Conclusion……………………………..…………………………………..86

Chapter 8 Conclusion……………………………………………...92

Reference……………………………………………………………94

Vita

Publication List

Table Captions

Chapter 5

Table 5.1 Extracted intrinsic parameters of a 0.08 μm × 100 μm InAs/InGaAs HEMT with different drain-source voltage V_{DS} from 0.5 to 0.9 V. ……………68

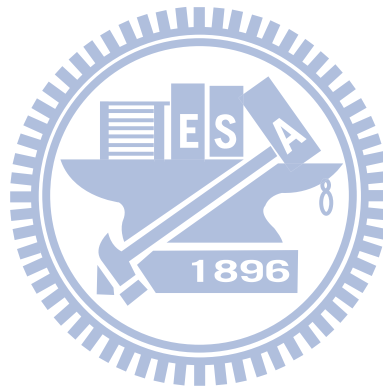

Figure Captions

Chapter 1

Fig. 1.1 Conventional HEMT structure……………………………………………..7

Fig. 1.2 Energy band gap v. s. lattice constant for $In_xAl_{1-x}As/In_yGa_{1-y}As$ system…….8

Fig. 1.3 Process flow of fabricating of 50-nm T-shaped gate using E-Beam lithography and tri-layer resist…………………………………………….9

Fig. 1.4 Cross sectional SEM image of the profile of tri-layer resist after E-beam lithography and development……………………………………………10

Fig. 1.5 Cross sectional SEM image of the 50-nm Ti/Au (10nm/30nm) T-shaped gate on InP substrate……………………………………………………..11

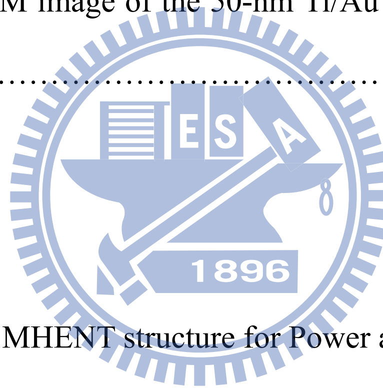

Chapter 2

Fig. 2.1(a) Double δ-doped MHENT structure for Power application………………19

Fig. 2.1(b) InAs-Channel HEMT for high-speed, low-power consumption applications………………………………………………………...20

Fig. 2.2 Mesa Etching…………………………………………………………..21

Fig. 2.3 Ohmic photo……………………………………………………………21

Fig. 2.4 Ohmic metal……………………………………………………………21

Fig. 2.5 Ohmic window and ebeam T-gate followed by recess………………………22

Fig. 2.6 Gate metal deposition…………………………………………………….23

Fig. 2.7 Passivation……………………………………………………………..23

Fig. 2.8 Nitride Via Etching………………………………………………………23

Fig. 2.9 TLM of the AuGe/Ni/Au Ohmic contact for MHEMT……………………..24

Fig. 2.10 (a) The TLM patterns, (b) The illustration of utilizing TLM to measure the Ohmic contact resistanc……………………………………………………25
Fig. 2.11 The First Photolithography for Plating Vias………………………………26
Fig. 2.12 Thin Metals Ti/Au Deposition……………………………………………..26
Fig. 2.13 The Second Photolithography for Plating Areas…………………………..26
Fig. 2.14 Au electroplating…………………………………………………………..27
Fig. 2.15 After thin metal etching and PR Removal………………………………27
Fig. 2.16 Photos of the Au airbridges of the device…………………………………28

Chapter 3

Fig. 3.1 Band diagrams at three different locations along the channel of a HEMT….43
Fig. 3.2 Actual characteristics and those predicted by Eq. (3-3)……………………44
Fig. 3.3 TLM pattern…………………………………………………………………..45
Fig. 3.4 The illustration of utilizing TLM to measure ohmic contact resistance……45
Fig. 3.5 The equivalent two-port network schematic at low frequency……………46
Fig. 3.6 The equivalent two-port network schematic at high frequency……………46
Fig. 3.7 Small signal representation of a common source FET……………………46
Fig 3.8 Definition of Cutoff Frequency f_T…………………………………….…47

Chapter 4

Fig. 4.1 Current-voltage characteristics of 0.07 × 80 μm^2 MHEMT………………52
Fig. 4.2 Two terminal gate-to-drain breakdown characteristics of 0.07 × 80 μm^2 MHEMT……………………………………………………………………..53
Fig. 4.3 Frequency dependence of current gain (H21) and MAG/MSG of power MHEMT…………………………………………………………………………54
Fig. 4.4 Noise figure (NF) of 0.07 × 80 μm^2 MHEMT measured from 1 to 16 GHz..55

Fig. 4.5 Measured 32 GHz power performance of 0.07 × 160 μm^2 power MHEMT at drain bias of 2.5 V……………………………………………………….56

Chapter 5

Fig. 5.1 (a) Output characteristics of a 0.08 μm × 100 μm InAs/InGaAs HEMT. Drain current I_D as a function of drain bias V_D with different gate voltage V_G from 0 V to -0.8 V. (b) Normalized output conductance g_o as a function of V_D of a 0.08 μm × 100 μm InAs/InGaAs HEMT………………………………….62

Fig. 5.2 (a) DC transconductance g_m of a 0.08 μm × 100 μm device as a function of V_G with different drain voltage V_D. (b) Plot of $|S_{21}|$ measured at 10, 30 and 60 GHz and g_m versus drain-source voltage of a 0.08 μm × 100 μm……...64

Fig. 5.3 (a) The gate current I_G plotted as a function of V_G at different V_D from 0 V to 1 V, 0.1 V per step. (b) Typical current gain $|h_{21}|$, MAG/MSG and U_g as a function of frequency of a 0.08 μm × 100 μm InAs/InGaAs HEMT. The V_{DS} is 0.7 V, the V_G is –0.4 V……………………………………………………….66

Chapter 6

Fig. 6.1 Layer structure of an InAs-channel HEMT grown by MBE on semi-insulating 2-in-diameter InP substrate………………………………………………74

Fig. 6.2 Current-voltage characteristics of 0.08 × 100 μm^2 InAs-channel HEMT…..75

Fig. 6.3 Typical current gain $|h_{21}|$, MAG/MSG and U_g as a function of frequency for a 0.08 × 100 μm^2 InAs-channel HEMT. V_{DS} is 0.7 V and the dc power is 22.3 mW…………………………………………………………………...….76

Fig. 6.4 Typical current gain $|h_{21}|$, MAG/MSG and U_g as a function of frequency for a 0.08 × 100 μm^2 InAs-channel HEMT for ultralow-power operation. V_{DS} is

0.2 V and dc power is 1.2 mW.Fig. 6.5 Comparison between the calculated and measured S-parameters under V_{ds} = 1.5V and V_{gs} = -0.6V……………77

Fig. 6.5 RF performance figures of merit as a function of dc power consumption for a $0.08 \times 100\ \mu m^2$ InAs-channel HEMT…………………………………...78

Fig. 6.6 Measured minimum noise figure and associated gain of a $0.08 \times 100\ \mu m^2$ InAs-channel HEMT from 2 to 18 GHz at V_{DS} of 0.2 V with a dc power dissipation of 1.2 mW…………………………………………………...79

Fig. 6.7 Measured minimum noise figure and associated gain of a $0.08 \times 100\ \mu m^2$ InAs-channel HEMT at 12 GHz as a function of dc power consumption at a higher V_{DS} of 0.5 V……………………………………………………..80

Fig. 6.8 Measured minimum noise figures and associated gains of a $0.08 \times 100\ \mu m^2$ InAs-channel HEMT at different V_{DS} from 0.1 V to 0.5 V with different total dc power dissipations at 12 GHz………………………………………………...81

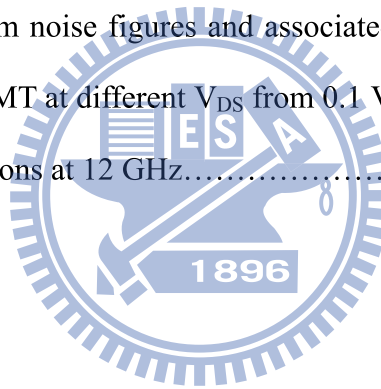

Chapter 7

Fig. 7.1 Schematic cross-sectional diagram of an InAs-channel MOS-HEMT with ALD Al_2O_3 gate dielectric…………………………………………………87

Fig. 7.2 (a) Extrinsic drain current and (b) transconductance versus gate bias for an 80-nm InAs-channel MOS-HEMT with 3-nm ALD Al_2O_3 gate dielectric at a V_{DS} of 0.7 V; (c) and (d) an for InAs-channel HEMT without gate dielectric……………………………………………………………………88

Fig. 7.3 Gate leakage current versus voltage for a conventional InAs-channel HEMT and InAs-channel MOS-HEMTs with 3-nm, 5-nm, and 7-nm ALD Al_2O_3 gate dielectric……………………………………………………………....89

Fig. 7.4 Measured minimum noise figure and associated gain (a) for an InAs-channel

MOS-HEMT from 20 to 60 GHz at V_{DS} of 0.6 V with a DC power dissipation of 4.9 mW and (b) for a conventional InAs-channel HEMT from at V_{DS} of 0.6 V with a DC power dissipation of 9 mW…………………….....90

Fig. 7.5 Typical current gain $|h_{21}|$, MAG/MSG and U_g as a function of frequency for an InAs-channel MOS-HEMT with 3-nm ALD Al_2O_3 at V_{DS} of (a) 0.3 V and (b) 0.7 V; for a conventional InAs-Channel HEMT without Al_2O_3 at V_{DS} of (c) 0.3 V and (d) 0.7 V respectively………………………………………..91